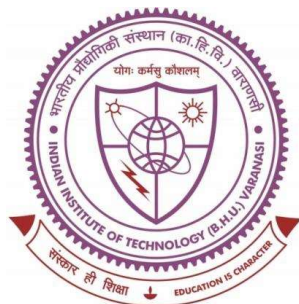


INVESTIGATIONS ON HYSTERESIS IN PEROVSKITE HALIDES FOR PHOTOVOLTAIC APPLICATIONS



THESIS SUBMITTED IN PARTIAL FULFILLMENT FOR THE AWARD OF
DEGREE

Doctor of Philosophy

In

Physics

By

PREM CHANDRA BHARTI

UNDER THE SUPERVISION OF

PROF. PRABHAKAR SINGH

DEPARTMENT OF PHYSICS

INDIAN INSTITUTE OF TECHNOLOGY

(BANARAS HINDU UNIVERSITY)

VARANASI – 221005

17171504

2024

Dedicated

To

My

Great – Grandfather

CERTIFICATE

It is certified that the work contained in the thesis titled "INVESTIGATIONS ON HYSTERESIS IN PEROVSKITE HALIDES FOR PHOTOVOLTAIC APPLICATIONS" by "PREM CHANDRA BHARTI" (Roll No. 17171504), in partial fulfillment of the requirement for award of degree of **Doctor of Philosophy** at **Indian Institute of Technology (B.H.U), Varanasi** is a record of his own work carried out under my supervision and guidance and this work has not been submitted elsewhere for a degree.

It is further certified that the student has fulfilled all the requirements of Comprehensive Examination, Candidacy, and SOTA for the award of Ph.D. Degree.

Date: 01/10/2024

Place: Varanasi



Co-Supervisor

Assistant Professor
(Dr. Sunil Kumar Singh)
Department of Physics
Indian Institute of Technology
(Banaras Hindu University)
Varanasi-221005



Supervisor
Dr. Prabhakar Singh

01/10/2024
Prof. Prabhakar Singh
Department of Physics
Indian Institute of Technology (BHU)
Varanasi-221005
(Department of Physics)

COPYRIGHT TRANSFER CERTIFICATE

Title of the Thesis: "Investigations on Hysteresis in Perovskite Halides for Photovoltaic Applications"

Name of the Student: Prem Chandra Bharti

Copyright Transfer

The undersigned hereby assigns to the Indian Institute of Technology (Banaras Hindu University) Varanasi all rights under copyright that may exist in and for the above thesis submitted for the award of the "*Doctor of Philosophy*".

Date: 01/10/2024

Place: IIT (BHU), Varanasi



Signature of the Student

(Prem Chandra Bharti)

Note: However, the author may reproduce or authorize others to reproduce material extracted verbatim from the thesis or derivative of the thesis for author's personal use provided that the source and the Institute's copyright notice are indicated.

Acknowledgments

Foremost, I would like to express my sincere gratitude to my supervisor Prof. Prabhakar Singh, Department of Physics, Indian Institute of Technology (Banaras Hindu University), for the continuous support to my Ph.D. study and research, for his patience, motivation, enthusiasm, and immense knowledge.

I would also like to express my sincere thanks to RPEC member's Dr. Sanjay Singh, School of Materials Science & Technology, Indian Institute of Technology (Banaras Hindu University), and Dr.P.C. Pandey, Indian Institute of Technology (Banaras Hindu University), for their encouragement, insightful comments, and stimulating help.

I wish to express deep regards to all the teachers of the Department Prof. Sandip Chatterjee, Prof. D. Giri, Prof. R. Prasad, Dr. P. C. Pandey, Dr. Shail Upadhyay, Dr. A. K. Srivastava, Dr. S. K. Mishra, Dr. S. K. Singh, Dr. Avani Singh Parmar, Dr. Saurabh Tripathi, Dr. Awaneesh Singh, Dr. R. K. Singh, Dr. Swapnil Patil, Dr. Shradha Mishra, Dr. Prasun Dutta, Dr. Rajeev Singh, Dr. Somnath Nag, Dr. Gauhar Abbas, Dr. Bidya Binay Karak, Dr. P. K. Aluri for their kind support at all moment during the progress of my research.

I would like to express my thanks to Dr. Pardeep K. Jha and Dr. Priyanka A. Jha, Department of Physics, IIT (BHU), Varanasi for their encouragement, guidance, support, and scientific approach in solving the difficulties faced during the research work.

My sincere thanks also go to CIFC, IIT (BHU), Varanasi for help in carrying characterization of the synthesized samples. I am also grateful to all office staff of the Department and authorities of IIT (BHU), for their kind help during the period of my stay to complete the thesis work.

With a special thanks to my senior Dr. Vani Pawar, Dr. Manish Kumar, Dr. Ajay S. Bangwal, Dr. Pragati Singh, Dr. Vandna Tomar, Dr. Varsha Yadav, Dr. Priyam Singh, Dr. Manisha Chauhan and my labmates, Mr. Rajeshwar Prasad, Dr. Uma Sharma, Mr. Ashish K Ranjan, Ms. Swarnima Singh, Ms. Manisha Shrama, Mr. Jay Narayan Mishra, Ms. Kamana Mishra, Mr. Hemant Kumar, Mr. Vishal Singh, Mr. Akash patel and Mr. Shivam Sharma for their support, suggestion, and healthy discussion of my research issues.

I would like to thank my coursework batchmates Dr. Bhagyasree Verma and Dr. Harshita Trivedi working with them during assignments and lab project was a wonderful moment.

I would like to thank my dearest friends from school, and college times, Mr. Sanjay Yadav, Mr. Shivam Yadav, Mr. Satyam Singh, Mr. Shashank Shekhar, Mr. Dheeraj Kumar, Dr. Puspendra Yadav, Dr. Maya Chauhan, Mr. Satya Vijay Kumar, Mr. Sudhir Kumar, Mr. Sawan Kumar, Mr. Dharmendra Kumar, Dr. Ranjeet Kumar, Dr. Yogesh Kumar and Mr. Shailendra Kumar for their support in my tough time.

I would like to express my deepest gratitude to my parents Mr. Sabhapati Bharti and Mrs. Sheela Devi for their unwavering love, and incredible support throughout this journey. I would like to extend my heartfelt thanks to my sisters Mrs. Chanda Bharti, Ms. Simpi Bharti, and Ms. Karishma Bharti for their boundless love and being my pillar of strength. To my little nephews, Mr. Akshansh and Mr. Ayansh, thank you for bringing so much joy and laughter to my life. Their innocent smiles, and playful energy have been a wonderful reminder to stay positive and keep pushing forward.

I would like to thank my wife Deepa Gautam for her constant support, limitless love, and endless understanding. Her presence and encouragement have been my greatest source of strength.

Last but not the least I would like to express my deepest gratitude to my great-grandfather, whose legacy continues to inspire me. I am honored to acknowledge his lasting influence on our family and on me personally.

Date:

Place: IIT(BHU) Varanasi

(Prem Chandra Bharti)

Contents

CERTIFICATE	v
DECLARATION BY THE CANDIDATE	vii
COPYRIGHT TRANSFER CERTIFICATE	ix
Acknowledgments	xi
Contents	xiii
LIST OF FIGURES	xix
LIST OF TABLES	xxvii
LIST OF SYMBOLS AND ABBREVIATIONS	xxix
PREFACE	xxxiii
CHAPTER 1: Introduction and Literature Survey	1
1.1 Present Energy Scenario.....	1
1.1.1 Global Energy Crisis	2
1.1.2 Possible Solutions of energy crisis:.....	3
1.1.3 Solar Energy- An Alternative Option.....	4
1.2 Working Principle of Solar Cell.....	8
1.3 Characteristics of Solar Cells	10
1.3.1 The current-voltage (I-V) characteristics	11
1.3.2 Open-Circuit Voltage (V_{oc})	12
1.3.3 Short-Circuit Current (I_{sc}).....	12
1.3.4 Maximum Power Output (P_{max})	13

1.3.5	Fill Factor (<i>FF</i>).....	14
1.3.6	Power Conversion Efficiency (<i>PCE</i>)	14
1.4	Generations of Solar Cell	15
1.4.1	First generation solar cells.....	16
1.4.2	Second generation solar cells	16
1.4.3	Third generation solar cells	18
1.5	Perovskite Crystal Structure, and Goldschmidt Tolerance Factor	19
1.6	Why Perovskites Solar Cell ?.....	20
1.7	Literture Survey on the Perovskite halide solar cell	21
1.7.1	Methyl ammonium Lead Iodide (MAPbI_3) Solar Cells	22
1.7.2	Formamidinium Lead Iodide (FAPbI_3) based solar cells.....	24
1.7.3	Mixed perovskite halide.....	27
1.7.4	Inorganic solar cells	28
1.7.5	Lead free perovskite solar cell	30
1.8	Issues with the Perovskite Halides Solar Cell.....	31
1.8.1	Stability Issues with Perovskites	31
1.8.1.1	Structural/Intrinsic Stability	32

1.9 Current –Voltage(J-V) Hysteresis	33
1.10 Motivation	35
1.11 The Objective Of Current Research	35
1.12 Plan of the Present Thesis	36
CHAPTER 2: Materials, Method, and Characterization Techniques.....	39
2.1 Overview	39
2.2 Description of the materials	39
2.3 Synthesis of Materials	40
2.3.1 Cold Sintering Method using the Solid State Reaction Method (SSR).....	41
2.4 Characterization Techniques	44
2.4.1 Thermogravimetric Analysis (TGA).....	44
2.4.2 Differential Scanning Calorimetry (DSC).....	47
2.4.3 X-Ray Diffraction (XRD)	49
2.4.4 Scanning Electron Microscope (SEM).....	53
2.4.5 Raman Spectroscopy	57
2.4.6 Ultra-Violet Visible (UV-Vis) Spectroscopy	61
2.4.7 Atomic Force Microscopy/ Piezoforce Microscopy (AFM /PFM)	66
2.4.8 DC Poling.....	70

2.4.9	Pyroelectric Effect.....	72
2.5	Electrical Properties	74
2.5.1	Current-Voltage ($I-V$).....	74
2.6	Impedance Spectroscopic Technique	76
2.7	Analysis Techniques	80
2.7.1	Rietveld Refinement Technique.....	80
2.7.2	Process of Analyzing the Obtained Data.....	84
2.8	Conduction Mechanisms	84
2.8.1	Poole-Frenkel	85
CHAPTER 3: Study of Hysteresis in Centrosymmetric Copper Lead Iodide.....		87
3.1	Introduction.....	87
3.2	Experimental Details.....	87
3.3	Results and Discussion.....	88
3.3.1	X-ray Diffraction and microstructural studies	88
3.3.2	Current-Voltage studies.....	94
3.3.3	Impedance Studies.....	100
3.3.4	Hopping (space charge) polarization.....	103
3.3.5	Conduction mechanism	110

3.4 Conclusion.....	111
---------------------	-----

CHAPTER 4: Study of Phase Transition & its Effects on Current Voltage Hysteresis in novel Copper Tin(II) Iodide..... 115

4.1 Introduction.....	115
-----------------------	-----

4.2 Experimental Details.....	116
-------------------------------	-----

4.3 Results and Discussion.....	117
---------------------------------	-----

4.3.1 Structural Prediction, Phase Transition and Hysteresis	117
--	-----

4.3.2 Ionic Conduction behaviour at phase transition.....	121
---	-----

4.3.3 Vibrational mode behaviour at phase transition.....	122
---	-----

4.4 Conclusion.....	125
---------------------	-----

CHAPTER 5: Study of Isomorphic Phase Transition in non-Perovskites Green CsSnI₃ and its impact on Hysteresis 127

5.1 Introduction.....	127
-----------------------	-----

5.2 Experimental Details.....	127
-------------------------------	-----

5.3 Results and Discussion.....	128
---------------------------------	-----

5.3.1 Structural study	128
------------------------------	-----

5.3.2 I-V Study	135
-----------------------	-----

5.3.3 AFM study.....	138
----------------------	-----

5.4 Conclusion.....	147
---------------------	-----

CHAPTER 6: Conclusions and Future Scopes 149
6.1 Conclusion of the Present Investigation..... 149
6.2 Outlook for Future Work..... 153
References 155
List of Publications 171

LIST OF FIGURES

Figure 1.1 Energy production from 2010 to 2050 using various energy sources [2].	1
Figure 1.2 Energy consumption and electricity generation over the previous year [3].	2
Figure 1.3 Reasons of energy crisis.	3
Figure 1.4 Different renewable energy sources.	4
Figure 1.5 Illustrates the spectrum of solar radiation [23].	5
Figure 1.6 The sun's angle determines solar irradiation	6
Figure 1.7 Angles describing the sun's position in the sky [20].	7
Figure 1.8 Determination of the Air Mass Index [27].	8
Figure 1.9 (a) shows the fundamental components of a solar cell[21] (b) symbolises architect of perovskite solar cell (c) The operational mechanism of a perovskite solar cell [32].	9
Figure 1.10 Equivalent circuit model of the solar cell[38].	10
Figure 1.11 Schematic representation of the I-V characteristics of a solar cell in both dark and light conditions[40].	11
Figure 1.12 Generations of the Solar Cell[47].	15
Figure 1.13 Arrangement of atoms in the perovskite substance [55].	20
Figure 1.14 Different technology power conversion efficiency trends from 1975 to 2024[59].	21

Figure 1.15 Current-Voltage hysteresis in PSC [170].	34
Figure 2.1 Flow chart of the cold sintering process for synthesizing perovskite samples.	43
Figure 2.2 Yellow precipitate of lead iodide (PbI ₂).	44
Figure 2.3 A thermogram curve showing the change of mass of a substance at different temperature [182].	46
Figure 2.4 (a) Depicting the schematic diagram of TGA[183] (b) Experimental setup of TGA at Central instrument facility IIT(BHU).	46
Figure 2.5 (a) Schematic diagram of DSC[185] (b) the experimental setup of DSC at CIF IIT (BHU).	48
Figure 2.6 Illustration of Bragg's law X-ray diffractometer.	51
Figure 2.7 Schematic representation of $\theta/2\theta$ diffraction in Bragg-Brentano geometry [189].	52
Figure 2.8 X-ray diffractometer (Rigaku-Miniflex II DESKTOP), Deapartment of Physics IIT (BHU).	53
Figure 2.9 The interaction of the electron beam with the sample [193].	54
Figure 2.10 (a) Working Principal of SEM [195] (b) Experimental setup of SEM measurement (CIF- IIT (BHU)).	56
Figure 2.11 (a) Components of raman spectrograph[197] (b) representation of the principle of Raman spectroscopy[198].	59
Figure 2.12 Experimental setup of LabRAM HR Evol Raman spectroscope.	60
Figure 2.13 Experimental setup of JASCO V-770 UV-Vis spectrometer	61

Figure 2.14 Tauc plot generated by Tauc equation.	63
Figure 2.15 Graphical representation of the valence and conduction bands and band tail (urbach energy) [201].	64
Figure 2.16 Estimation of Urbach energy	65
Figure 2.17 Basic concept of PFM, (a) downward polarization and (b) upward polarization of ferroelectric domains[204].	69
Figure 2.18 (a) Block diagram [205] (b) experimental set up of AFM/PFM at CIF(IITBHU).....	69
Figure 2.19 Random alignment of dipoles before poling(left) and single order alignment of dipole after poing(right) [206].	70
Figure 2.20 (a) Schematic of dc poling unit [207] (b) experimental setup of dc poling unit	71
Figure 2.21 An illustration of a pyroelectric generator concept[210].	73
Figure 2.22 Pyroelectric measurement system (Keithely 6517B electrometer)	73
Figure 2.23 An experimental setup of a solar simulator with a Keithley source meter.....	74
Figure 2.24 The frequency response of the equivalent circuit and its complex impedance plot.	78
Figure 2.25 Represents the experimental Solartron 1260 A impedance analyzer with sample holder and furnace	79
Figure 3.1 (a) XRD pattern of sample sintered at 5, 30, 100, 150 and 200 °C (abbreviated as T1, T2, T3, T4 and T5 respectively), (b) Le-bail fit of XRD of T3 sample with R3m symmetry (major peaks indexed), (c) 21R prototype of the R3H layered hexagonal crystal structure, (d) Variation of	

lattice parameters a, b and c with the sintering temperature and (e) Variation of grain size with the sintering temperature.....	89
Figure 3.2 Raman spectra of powder CuPbI ₃ synthesized at RT with wavelength $\lambda_{exc} = 532$ nm	90
Figure 3.3 Rietveld refined spectrum of X-ray diffractograms of CuPbI ₃ synthesized at 100 °C with R3m symmetry.....	91
Figure 3.4 SEM micrographs and grain size histograms for the estimation of grain size.....	94
Figure 3.5 Time scale: AM 1.5G sun light applied to samples, the arabic numerical (1–8) represent the sequential point on time scale at which IV measurement has been taken. IV curves for sample sintered at 5, 30, 100, 150 and 200 °C (abbreviated as T1, T2, T3, T4 and T5 respectively) (b) in dark (point 1 on time scale) and (c) In light (point 8 on time scale),.....	95
Figure 3.6 (a) The I–V curves for dark and just illuminated (b) AHys with voltage for the studied samples (c) second order derivative with voltage (d) variation of extracted parameters ‘n’ (lines are to guide only) from fitting $J = kE^n$ for both dark and light (e) variation of ΔA_{Hys} with the grain size (f) variation of activation energy with the sintering temperature.	96
Figure 3.7 Fitting of I-V characteristics in dark and light with the relation $I = kV^n$	98
Figure 3.8 Arrhenius plots for estimation of activation energy using Gibbs’ free energy.....	98
Figure 3.9 Band gap estimation using UV-visible spectroscopy.	99
Figure 3.10 (a) Impedance spectra (for ac voltage amplitude 1 V) before and after light with the grain size showing disintegration of grain–boundary, (b) Bode plot of imaginary part of permittivity with the oscillation amplitude for T2 and T3 sample, (c) Gaussian fitting of T2 and T3 sample at	

small oscillation amplitude 0.25 V before and after light and (d) relaxation time for T2 and T3 sample before and after light in grain and grain–boundary regime	101
Figure 3.11 : Fitting of Imaginary part of Impedance using Gaussian function with oscillation amplitude for T2 sample in dark.....	102
Figure 3.12 Frequency dispersion (relative) permittivity curves for the T2 and T3 samples in pristine and after light fall conditions.....	104
Figure 3.13 : Fractal exponent in BCP using relation $ Z = f^{-\alpha}$ for (a) grain and (b) grain boundary of pristine and after light sample, where $\alpha = 0$ for pure resistive, $\alpha = 1$ for pure capacitive and $\alpha = 0.5$ corresponds to diffusion limited bound transport in a layer. However, $\alpha = 0.35$ describes the conduction with the hindrances of the host matrix and increase in the value of α from 0.5 to 0.8 suggest increased surface accumulation of charge carriers as illustrated by (c) scheme for the T2 and T3 samples in Dark and AM 1.5 G sun light	107
Figure 3.14 Plot of $\log z $ vs $\log f$ with oscillation amplitude for T2 sample in dark	107
Figure 3.15 Plot of $\log z $ vs $\log f$ with oscillation amplitude for T2 sample in light.....	108
Figure 3.16 Plot of $\log z $ vs $\log f$ with oscillation amplitude for T3 sample in dark.	109
Figure 3.17 Plot of $\log z $ vs $\log f$ with oscillation amplitude for T3 sample in light.	109
Figure 3.18 Frenkel poole curves and (b) variation of relative dielectric constant for the T2 and T3 samples in dark and AM 1.5 G sun light	110
Figure 4.1 a) XRD b) crystal structure, c) band gap estimation from Tauc plots (inset) UV absorbance curve with wavelength, d) DSC curves	118

Figure 4.2 a) I-V Curve for Pristine and Poled sample in dark and light (AM 1.5 G) condition at 300 K (inset) suggest in Poled sample hysteresis area (A_{Hys}) reduced in light while in case of Pristine sample, A_{Hys} is greater as compare to dark. b) I-V Curve for Pristine and Poled sample in dark and light at 298 K, 313 K, 333 K and 353 K c) variation of A_{Hys} with temperature in dark and light conditions..... 119

Figure 4.3 Temperature dependent conductivity measurements at different frequencies..... 120

Figure 4.4 J-P law fitting in pristine $CuSnI_3$ 122

Figure 4.5 The variation of parameters a) dc conductivity(σ_{dc}), b) hopping frequency (ω_H) and c) frequency exponent (s) with temperature..... 123

Figure 4.6 High temperature Raman spectra of $CuSnI_3$ 124

Figure 4.7 Variation of a) normalised intensity with wave number for A and E modes at different temperatures b) mode corresponding tp Raman shift ω_1 and ω_2 with temperature 125

Figure 5.1 (a) XRD of green $CsSnI_3$ along with the reported JCPDS of orthorhombic- $CsSnI_3$ for Black (B- γ) and Yellow(Y- γ) polymorph, (b) Raman spectra with 633 nm and 785 nm laser, (inset) colour patterns representing the colour polymorphs of $CsSnI_3$ on phase symmetry axis, suggesting the G- $CsSnI_3$ possess high symmetry than B- γ and Y- γ polymorphs (c) Variation of absorbance and Tauc plot showing the band gap of 1.24 eV cold-sintered green $CsSnI_3$ 129

Figure 5.2 (a) Rietveld refinement of G- $CsSnI_3$ with cubic $Pa\bar{3}$ symmetry (b) electron density (Patterson) maps (c) Crystal Structure showing Z = 8 (d) Bond angle with bond length. 131

Figure 5.3 : (a) Temperature dependent (i) second derivative of heat (from DSC) and (ii) dielectric study in the range of (250–460 K) with comparative of phase transition in existing B- and Y- $CsSnI_3$ (two panels yellow and black at top) with possible transitions in G- $CsSnI_3$ (bottom panel).

(Symbol & Abbreviations: ×(*Red*)-room temperature (here temperature at which characterization is performed), w-weak, vw-very weak) (b) inverse group (*G*)-subgroup (*H*) relation tree for the minimal supergroup of Pa3 the possible sequence of successive isomorphic phase transitions ($Pm\bar{3}m \rightarrow Pm\bar{3} \rightarrow Ia\bar{3} \rightarrow Pa\bar{3}$) with decrease in temperature is shown by dashed line (inset: green CsSnI₃ powder)..... 134

Figure 5.4 a) The I –V curves for dark and just illuminated, at 298 K, 313 K, 333 K and 353 K (b) A_{Hys} plot (c) Pyroelectric current Vs Temperature plot..... 136

Figure 5.5 a) voltage-time curve, b) normalised charge-time over a complete cycle..... 137

Figure 5.6. a) PFM and a resistive switching imaged by C-AFM. A change in PFM contrast correlates with the transition from low current (dark contrast) to high current (bright contrast) at 298 K but no alteration in PFM amplitude and phase is appearing suggesting absence of ferroelectric phase (b) Amplitude and (c) Phase variation with voltage 139

Figure 5.7 Impedance bode plots in the pristine sample, after light (AL) treatment and after poling (AP) I-V measurement. 140

Figure 5.8 a) Fractal exponent variation with temperature for pristine, after light and freezed samples, (b) Variation of relaxation time with temperature for the studied samples (c) Ghosh scaling for the freezed charge carrier sample 141

Figure 5.9 Havriliak–Negami (HN) fitted permittivity bode plots for pristine sample, after light (AL) treatment (IV measurement) and after poling (AP). 142

Figure 5.10 Ghosh scaling for pristine sample, and after light (AL) I-V measurement..... 143

Figure 5.11 Raman spectrum with the variation of temperature for CsSnI₃ We have observed (B⁺₂)₃, tr, E⁺₂, F⁺, A⁺ and F⁺ marked at positions ω₁, ω₂, ω₃, ω₅ and ω₆, respectively correspond to Sn-I. Further, E_g modes corresponding to Cs-I bond are marked at ω₄ and ω₇. 144

Figure 5.12 Raman shift with variation Temperature 144

Figure 5.13 FWHM Raman peaks with variation of Temperature 145

LIST OF TABLES

Table 1.1 1 st generation photovoltaic cells.....	16
Table 1.2 2 nd generation photovoltaic cells.....	17
Table 1.3 3 rd generation photovoltaic cells.....	18
Table 2.1 Specifications of the raw materials.....	40
Table 3.1 Parameters used to obtain fitting but failed	92
Table 3.2 Parameters used to obtain fitting.	93
Table 3.3 Relaxation parameters for pristine sample.....	105
Table 3.4 Relaxation parameters for sample after light fall.....	105
Table 5.1 Wyckoff positions, atomic positions for G-CsSnI ₃	132
Table 5.2 Anisotropic Thermal Parameters (\AA^2)	132
Table 6.1 Distribution of relaxation time in different samples after poling and after light fall	152

LIST OF SYMBOLS AND ABBREVIATIONS

PH	Perovskite Halide
PV	Photovoltaics
VB	Valence Band
CB	Conduction band
I_{sc}	Short Circuit Current
J_{sc}	Current Density
V_{oc}	Open Circuit Voltage
P	Power
P_{max}	Maximum Power Output
P_{in}	Power Incident
FF	Fill Factor
PCE (η)	Power Conversion Efficiency
R_s	Series Resistance
R_{sh}	Shunt Resistance
I-V	Current – Voltage
I_0	Reverse Saturation Current
I_L	Photo-generated Current
I_m	Maximum Current
V_m	Maximum Voltage
AM	Air Mass
DSSC	Dye-Sensitized Solar Cell
PSC	Perovskite Solar Cell
MA	Methyl ammonium
FA	Formamidinium
ETL	Electron Transport Layer

EDAI	Ethylenediammonium Iodide
TFEA	Trifluoroethylamine
AVAI	Aminovaleric acid Iodide
MDMC	Mixed Dimensional and mixed Compositional
HTL	Hole Transport Layer
HTM	Hole Transport Material
SCLC	Space Charge Limited Current
EDX	Energy Dispersive X-Ray Analysis
E_g	Band Gap
$h\nu$	Photon Energy
E_u	Urbach Energy
eV	Electron volt
meV	Mili electron Volt
FWHM	Full width at half maximum
g	Gram
K	Kelvin
M.P.	Melting Point
JCPDS	Joint Committee on Powder Diffraction Standards
LED	Light Emitting Diode
ΔG	Gibbs Free Energy
ΔS	Entropy
ΔH	Enthalpy
RT	Room Temperature
Å	Angstrom
mg	milligram
N	Avogadro's number
cm	Centimeter

μm	Micro-meter
W/m^2	Watt per meter square
mV	mill volt
nm	nanometer
SSR	Solid State Reaction
SEM	Scanning Electron microscope
UV-Vis	Ultraviolet-Visible
DSC	Differential Scanning Calorimetric
XRD	X-ray Diffraction
DMF	Dimethylformamide
DI	Deionized



PREFACE

Renewable energy sources, such as solar and wind power, must supplant traditional energy supplies, such as coal and petroleum, in order to preserve our planet. Among renewable energy sources, solar power is likely the most common. Therefore, solar energy has the potential to greatly benefit both the climate and the economies of rich and developing nations in the future when paired with a clean and sustainable energy source. Solar cells that generate electricity through photovoltaic (PV) technology appear to be a promising method of converting sunlight into electricity.

Solar cell materials have been the subject of extensive research over the last few decades. Since the inception of the first solar cell concept (PN junction) using crystalline Silicon solar cells, which achieved efficiency at US Bell Laboratories in 1954, it gained significant interest. The efficiency of amorphous silicon-based solar cells with multiple-junction manufacturing cells has ranged from 4 . Polycrystalline/monocrystalline Si solar cells have attained a photovoltaic conversion efficiency of above twenty percent. Which is now commercially accessible. Due to their high efficiency, the PV market is now dominated by Si-based solar cells. As a result, the materials that are currently known for their practical applications in solar cell technology are still based on silicon technologies. There is a significant demand for alternative solar cell materials that are highly efficient in enhancing the efficiency of silicon technology. However, the downsides of Si-based solar cells include rigorous preparation conditions and high costs. Additionally, technologies such as CIGS and CdTe thin film solar cells have exhibited exceptional power conversion efficiency (η); however, their commercial applications are impeded by environmental contamination, high production costs, and other

complications. An essential criterion for selecting a material for solar cell application is its durability, which should be approximately 25 to 30 years. A more cost-effective method of producing tunable perovskite semiconductors is available, in contrast to the expensive procedure required to produce silicon. Perovskite exhibits numerous advantages compared to prevailing silicon panels. Nevertheless, Perovskites have attracted researchers because of their resilient optoelectronic properties and exceptional photovoltaic capabilities. ABX_3 is the general formula for organic-inorganic halide perovskite. Here, $A = Cs^+, Cu^+$, $MA = CH_3NH_2^+$, $FA = HC(NH_2)_2^+$, $B = Pb^{2+}, Sn^{2+}, Ge^{2+}$, and $X = Cl, Br, \text{ or } I$. The first application of perovskite absorbers was documented in 2009. At that time, the efficiency rating of these cells was less than 4%, which was not particularly impressive. Furthermore, their durability was severely limited, making them unsuitable for practical applications. Because of these shortcomings, early perovskite solar cells failed to capture the attention or interest of researchers and scientists looking for more promising and efficient alternatives in photovoltaic technology. The scientific community consequently paid little attention to these early efforts using perovskite absorbers. Perovskite materials have drawn much attention because of their low cost and high potential in solar cell applications. Perovskite solar cells initially exhibited only modest power conversion efficiency (η). Nevertheless, scientists have made substantial progress in enhancing their performance through extensive research and technological advancements. Currently, the power conversion efficiency (η) of perovskite solar cells has surpassed 26%. Nevertheless, organic-inorganic halide perovskites are experiencing thermal instability as a result of the volatilization of organic cations that are present in the perovskite compositions. Perovskite lead halides have demonstrated their utility as outstanding optoelectronic devices, with band gaps between 1.3 and 2.3. This is attributed to their high absorption coefficient and the

elimination of the liquid hole transport layer, particularly in the context of dye-sensitized solar cell materials. Applications in optoelectronics and photovoltaics have shown significant interest in the cesium lead halides, denoted by the formula CsPbX_3 (where $X = \text{I}$ and Br). The direct bandgap nature of cesium lead halide compounds, along with their substantial light-absorbing capability in both the ultraviolet and visible spectrums, demonstrates their usefulness for solar cell applications. Additionally, these materials are utilized in applications, including light-emitting diodes (LED), photodetectors, and energy storage solutions. But, the major disadvantage of these materials is that they are too prone to moisture and degrade very fast. Hence, although these compounds possess notable optoelectronic characteristics, ensuring their stability is a crucial matter that must be addressed. Aside from compositional variation, several approaches are used to synthesize these materials in the air to address stability difficulties, such as solvothermal synthesis, quantum dots, one-step microwave-assisted, low-temperature synthesis, and solution phase synthesis. Therefore, it is imperative to comprehend the reasons for these materials' instability and their difficulty synthesizing them in ambient conditions. If it is intrinsic instability, it would not have been synthesized through the conventional solid-state route (SSR). But, in this thesis work, perovskite halides are nucleated at room temperature just by mixing the precursors, and that too in ambient conditions; thus, there is no need for calcination. The grain growth occurs after sintering the pellet in the vacuum at 80 for one hour (the synthesis details are provided in the experimental section). Therefore, this effortless cold sintering method was considered worthwhile for synthesizing the samples.

The main purpose of this thesis is to examine the current-voltage hysteresis issue in perovskite halides. Inorganic halide-based perovskite (CuPbI_3 , CuSnI_3 , and CsSnI_3) was chosen as the active material for this purpose. The I-V hysteresis of the samples has been

examined by altering the grain size by varying the sintering temperature and polarisation using DC poling.

The thesis has been divided into six chapters, each of which is described below:

Chapter 1: This chapter provides an overview of solar cells, including comprehensive reviews of existing literature. It analyzes the factors that drive work motivation, the historical context, and the basic principles of solar cells. It also highlights the necessary characteristics of active materials for perovskite solar cells. Furthermore, literature studies have identified significant perovskite halides (active materials) challenges. The chapter describes the current-voltage hysteresis problem in perovskite solar cells. This chapter also addresses the primary goals of the current study.

Chapter 2: This chapter explains the various experimental methods used in the current study. It describes the experimental equipment, analysis procedures, and synthesis routes used to produce the samples. The suggested system was synthesized using cold sintering procedures via a solid-state reaction process. It also provides a comprehensive overview of critical analytical techniques, including Rietveld refinement analysis. Additionally, it gives a detailed description of a variety of instruments, including XRD, SEM, TGA, DSC, UV-visible, AFM/PFM, DC Poling Unit, Electrometer for Pyro-current Measurement, Raman, impedance spectroscopy, and I-V measurement.

Chapter 3: this chapter aims to investigate the change in polarisation behaviour at the surface/interface of CuPbI_3 before and after light exposure. By altering the polarisation mechanism by varying the sintering temperature, compound CuPbI_3 was synthesized through the cold sintering technique. We also predicted the structure of CuPbI_3 . Further, the chapter

will explore the effects of light exposure on CuPbI_3 hysteresis area and shape, impedance analysis, and conduction/hopping mechanisms.

Chapter 4: Due to environmental concerns and lead toxicity, there has been significant interest in developing lead-free alternatives such as Lead-free perovskite halides tin-based (Sn) perovskites. This chapter investigates the photo hysteresis behavior and the impact of phase transitions on the hysteresis of the lesser-known lead-free compound CuSnI_3 . Lead-free halides perovskite CuSnI_3 was synthesized using the cold sintering method. Further, to investigate the impact of potential phase transitions on current-voltage hysteresis, we examined the temperature-dependent behavior of the current-voltage curve in both dark and light conditions, specifically in the presence of probable anomalies or phase transitions, such as AM 1.5 G. To observe the inherent characteristics of these irregularities, we subjected the sample to an electric field of 0.5 kV for a duration of 30 minutes. We then compared the current voltage behavior of the sample with its original state at a temperature of 300 K under normal environmental conditions.

Chapter 5: This chapter describes the isomorphic phase transition in the green polymorph of CsSnI_3 (G- CsSnI_3), which is cubic (Pa) at 295 K and persists in phase transitions at higher temperatures. We used PFM, temperature-dependent dielectric measurements, impedance spectroscopy, and Raman spectroscopy. To investigate the impact of the phase transition on current-voltage hysteresis, we examined the temperature-dependent behavior of the current-voltage curve under dark and light conditions (AM 1.5 G) around the phase transition. The poling impacts both domain size and grain number. Light and poling both appear to affect the relaxation time, which changes over transitions.

Chapter 6: This chapter concludes the findings of this research outcome and lists a few possibilities for future investigations.